

## Synergetic Enhancement of Light-Matter Interaction by Nonlocality and Band Degeneracy in ZnO Thin Films

Takashi Kinoshita,<sup>1</sup> Takuya Matsuda,<sup>1,\*</sup> Takuya Takahashi,<sup>2</sup> Masayoshi Ichimiya,<sup>3</sup> Masaaki Ashida,<sup>2</sup> Yoshiaki Furukawa,<sup>4</sup> Masaaki Nakayama,<sup>4</sup> and Hajime Ishihara<sup>1,2,†</sup>

<sup>1</sup>*Department of Physics and Electronics, Osaka Prefecture University, Sakai, Osaka 599-8531, Japan*

<sup>2</sup>*Department of Materials Engineering Science, Osaka University, Toyonaka, Osaka 560-8531, Japan*

<sup>3</sup>*Department of Electronic Systems Engineering, The University of Shiga Prefecture, Hikone, Shiga 522-8533, Japan*

<sup>4</sup>*Department of Applied Physics, Osaka City University, Osaka, Osaka 558-8585, Japan*



(Received 5 December 2018; revised manuscript received 8 March 2019; published 19 April 2019)

This study aims to reveal the full potential of ZnO as an ultrafast photofunctional material. Based on nonlocal response theory to incorporate the spatially inhomogeneous quality of the samples coupled with experimental observations of linear and nonlinear optical responses, we establish the ultrafast radiative decay of excitons in ZnO thin films that reaches the speed of excitonic dephasing at room temperature in typical semiconductors at a couple tens of femtoseconds. The consistency between the observed delay-time dependence of the transient-grating signals and the theoretical prediction reveals that the ultrafast radiative decay is due to the synergetic effects of the giant light-exciton interaction volume and the radiative coupling between multicomponent excitons.

DOI: [10.1103/PhysRevLett.122.157401](https://doi.org/10.1103/PhysRevLett.122.157401)

ZnO is one of most fascinating materials for a great source of atypical electronic properties [1,2], and also for optoelectronic devices, because of a very slow sample deterioration, a wide band gap, and high excitonic stability [3,4]. In particular, its large exciton binding energy ( $\sim 60$  meV) is far greater than the thermal energy at room temperature, making the material suitable for various photonic applications, including light-emitting diodes [5–7], ultraviolet photovoltaics [8,9], and exciton-polariton lasing [10–12]. Thus, ZnO will continue to be a leading material in future photonic technologies. However, unveiling the key mechanisms of the high-performance photofunctions and the full potential of this material is currently a core challenge.

Recently, it was theoretically predicted that excitonic radiative decay rate is greatly enhanced by the synergetic effects of the giant light-matter interaction volume with nonlocal response and the radiative coupling of multicomponent excitons due to near degeneracy in the top valence bands of ZnO [13,14]. Regarding the former effect, it is known that in a nano-to-bulk crossover size regime, an unconventional wave-wave coupling beyond the long wavelength approximation (LWA) regime is activated through spatial interplay between multipole excitonic waves and light waves [15–17]. This strong coupling leads to drastic radiative corrections (i.e., energy shifts and radiative widths) in the order of several tens of meV [18,19]. Regarding the latter effect, it has recently been clarified that the radiation-induced coupling between *A* and *B* excitons in ZnO causes bright and dark modes, and that bright modes dominate the radiative width. This effect further speeds up the radiative decay of ZnO excitons.

The predicted radiative decay with a few tens of femtoseconds [13,14] is an order of magnitude faster than the recently recorded ultrafast radiative decays with a couple of hundred femtoseconds [18–23]. The realization that the predicted speed is faster than the thermal dephasing is significant because it would greatly reduce the thermal energy loss in optical operations. We aim to determine whether such a short radiative decay time comparable to the excitonic dephasing time at room temperature [24] can be realized in real samples. In reality, the crystalline quality is usually inhomogeneous due to various types of impurities and defects, even in those fabricated with state-of-the-art technology. This risks spatially modifying the excitonic wave functions and affecting the coherent optical response. In this work, we employ the theoretical method to incorporate such possible sample modifications, and deduce the spatially varying nonradiative damping of excitons by comparing the theoretical results with the observed linear (reflectance) and nonlinear [three-pulse degenerate four-wave mixing, that is, transient grating (TG)] optical responses. We measured the time profile of TG at the theoretically calculated eigenenergies of the light-exciton coupled system, directly providing information regarding pure population relaxations [25–27]. The agreement between the theoretical and experimental results establishes the extremely fast radiative decay of a couple of tens of femtoseconds due to the giant light-exciton interaction volume and the radiative coupling of *A* and *B* excitons even in realistic samples that are inhomogeneous.

To introduce a spatial modulation of the excitonic coherence in the calculation, we discretized the medium

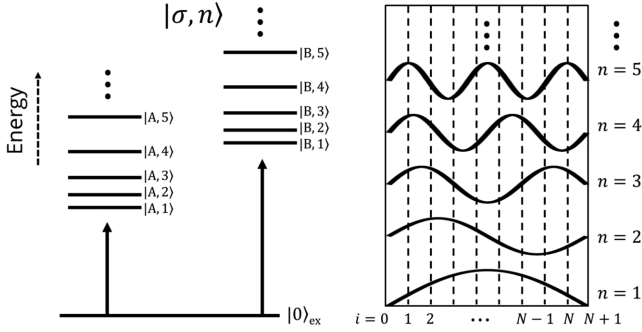


FIG. 1. (left) Energy diagram and (right) wave functions of A and B excitons.  $\sigma$  and  $n$  are indices to label exciton components ( $\sigma = A$  or  $B$ ) and size-quantized states, respectively.

into  $N$  layers with a small interval  $a$  (we fixed  $a = 0.5$  nm), as shown in Fig. 1. The value of  $a$  is approximately the same as the lattice constant along the  $c$  axis of ZnO. The in-plane direction is assumed to have translational symmetry. For the sufficiently large excitonic bandwidth (i.e., large transfer energy), this discretized model provides essentially the same result as that by the continuum model [13] with the effective-mass parameter appropriately converted from the transfer parameter given in Eq. (2). Excitons in ZnO fit this case well. The reduced density operator  $\rho(t)$  satisfies the following Lindblad-type master equation [28]:

$$\frac{\partial}{\partial t}\rho(t) = \frac{1}{i\hbar}[\mathcal{H}_S, \rho(t)] + \frac{1}{\hbar} \sum_i \Gamma_{\sigma,i} (2\beta_{\sigma,i}\rho(t)\beta_{\sigma,i}^\dagger - \{\beta_{\sigma,i}^\dagger\beta_{\sigma,i}, \rho(t)\}), \quad (1)$$

where  $\sigma$  is an index to label exciton components ( $\sigma = A$  or  $B$ ),  $i$  is a site index, and  $\beta_{\sigma,i}$  ( $\beta_{\sigma,i}^\dagger$ ) is an annihilation (creation) operator of an exciton.  $\Gamma_{\sigma,i}$  denotes the coupling strength between the  $\sigma$  exciton and a thermal bath, e.g., phonon, impurity, defects, and so on. Excitons lose their spatial coherence through the parameter  $\Gamma_{\sigma,i}$ .

The system Hamiltonian  $\mathcal{H}_S$  is written as

$$\mathcal{H}_S = \epsilon_\sigma \sum_i \beta_{\sigma,i}^\dagger \beta_{\sigma,i} - t_\sigma \sum_i (\beta_{\sigma,i+1}^\dagger \beta_{\sigma,i} + \beta_{\sigma,i}^\dagger \beta_{\sigma,i+1}) - \sum_i \sum_\sigma \mu_\sigma (\beta_{\sigma,i}^\dagger + \beta_{\sigma,i}) \mathcal{E}_i(t), \quad (2)$$

where  $\epsilon_\sigma$  denotes the energy of the  $\sigma$  exciton at each site,  $t_\sigma$  is the transfer energy between neighboring sites originating from the excitonic nonlocality whose value relates to the effective-mass of an exciton  $M_\sigma$  as  $t_\sigma \approx \hbar^2/(2M_\sigma a^2)$  around the small wave number region, and  $\mu_\sigma$  is the coupling strength between an exciton and an electric field  $\mathcal{E}_i(t)$  whose value relates to the longitudinal-transverse (LT) splitting energy  $\Delta_{LT}^\sigma$  [13]. The third term of the right-hand side in Eq. (2) indicates the light-matter interaction

which induces a mixing of different-component excitons via radiation fields through the sum over  $\sigma$ .

The trace is performed over all one-exciton states  $\beta_{\sigma,i}^\dagger |0\rangle_{\text{ex}}$ , where  $|0\rangle_{\text{ex}}$  is a vacuum state of the exciton system. In the calculation, we used a commutation relation for bosons considering the linear optical response. In addition, assuming the system is close to a pure state, it is approximately used as  $\text{Tr}_S[\rho(t)] \approx 1$ .

We assume the incident lights are close to a normal incidence. Because the interval  $a$  is much shorter than the wavelength of light, the Fourier component of  $\mathcal{E}_i(t)$  approximately satisfies the discretized Maxwell equation under the normal incidence, given as

$$\tilde{\mathcal{E}}_i(\omega) = \tilde{\mathcal{E}}_i^{(0)}(\omega) + 4\pi a \left(\frac{\omega}{c}\right)^2 \sum_{\sigma'} \sum_{i'} \mu_{\sigma'} G_{i,i'}(\omega) \langle \beta_{\sigma',i'} \rangle(\omega), \quad (3)$$

where  $c$  is the velocity of light in a vacuum,  $\tilde{\mathcal{E}}_i^{(0)}(\omega)$  is the background electric field, and  $G_{i,i'}(\omega)$  is a discretized Green's function for the Maxwell equation in thin film structures [29] including contributions of nonresonant polarizations.  $\langle \beta_{\sigma,i} \rangle(\omega) \equiv (2\pi)^{-1} \int \text{Tr}_S[\rho(t)\beta_{\sigma,i}] e^{i\omega t} dt$  is a Fourier component of an expectation value of  $\beta_{\sigma,i}$  determined by solving Eqs. (1)–(3) self-consistently. Then, a closed linear equation set is obtained as

$$F_{\sigma,i}^{(0)}(\omega) = \sum_{\sigma'} \sum_{i'} [(\epsilon_\sigma - \hbar\omega - i\Gamma_{\sigma,i})\delta_{\sigma,\sigma'}\delta_{i,i'} - t_\sigma \delta_{\sigma,\sigma'} (\delta_{i',i-1} + \delta_{i',i+1}) + Z_{\sigma\sigma'ii'}(\omega)] \langle \beta_{\sigma',i'} \rangle(\omega), \quad (4)$$

where  $F_{\sigma,i}^{(0)}(\omega) = \mu_\sigma \tilde{\mathcal{E}}_i^{(0)}(\omega)$  indicates an interaction between the  $\sigma$  exciton and the background electric field at site  $i$ , and  $Z_{\sigma\sigma'ii'}(\omega)$  denotes the radiation-induced coupling between the  $\sigma$  exciton at site  $i$  and  $\sigma'$  exciton at site  $i'$  given as  $Z_{\sigma\sigma'ii'}(\omega) = -4\pi a(\omega/c)^2 \mu_\sigma \mu_{\sigma'} G_{i,i'}(\omega)$ . The nonlocal form of this term derives from propagation of the radiation field, while that of the terms relating to the transfer energy  $t_\sigma$  on the right-hand side of Eq. (4) comes from the excitonic nonlocality. These two nonlocalities are intertwined when the system length is comparable to the wavelength of light.

For the experiments, ZnO thin films with two different thicknesses were respectively grown on a (0001)  $\text{Al}_2\text{O}_3$  substrate by pulsed laser deposition using the fourth harmonic of an Nd:YAG laser with a repetition rate of 10 Hz and power density of 2.5 J/cm<sup>2</sup> [30]. A commercially supplied ZnO sintered body with a purity of 99.99 percent was used as a target. Oxygen was also used as atmosphere gas with a pressure of 1.33 Pa. The background pressure of the vacuum chamber was  $1.0 \times 10^{-7}$  Pa. The growth temperature and rate were set to 650 °C and

0.3 nm/s, respectively. The surface root mean square roughness of the grown films measured by an atomic force microscope was approximately 0.5 nm. We confirmed from x-ray diffraction patterns that the ZnO films are just oriented along the  $c$  axis. In the photoluminescence spectrum at 10 K measured with an He-Cd laser (325 nm), the spectral width of the neutral-donor-bound exciton line is less than 4 meV. The green band due to lattice defects is hard to observe, and the intensity is suppressed by 3 orders of magnitude compared to that of the bound exciton line.

The grown films were mounted in a helium-flow cryostat and cooled to 5 K. TG was measured using the second harmonic of a mode-locked Ti:sapphire laser with a repetition rate of 80 MHz. The pulse duration was accurately estimated to be 170 fs by the correlation between the fundamental and the second harmonics of the laser. The photon energy of the pulse was tuned to approximately the transverse  $A$  exciton energy in a ZnO bulk crystal (3.3780 eV) and the spectral width was approximately 25 meV, covering the exciton resonance region. The light was split into three pulses. All of them were focused onto the same spot and the two pump pulses were simultaneously injected on the sample surface. The polarizations of the two pump pulses were parallel, and the polarization of the probe pulse was perpendicular to that of the pump pulses. The sign of the delay time is defined as positive when the pump pulses precede the probe pulse. The signal light was detected in the backward diffraction geometry through an optical fiber to a monochromator equipped with a CCD. The spectral resolution was better than 0.10 meV. We designed two ZnO thin films that were 200 and 290 nm thick in the deposition process (the error of the thickness was within 10%), and the thickness at the measured spot in each film was estimated by fitting to the reflection spectrum measured using the same geometry and excitation light as those in the measurement of TG.

Figures 2(a) and 2(b) show the fitting of the observed reflectance spectrum. We modeled the position dependence of  $\Gamma_{\sigma,i}$  to reproduce the detailed peak structures, as shown in Figs. 2(c) and 2(d). From the fitting, we determined the

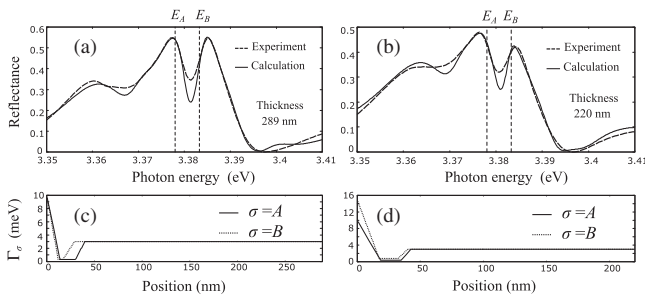


FIG. 2. Fitting of the observed reflectance for (a) 289 and (b) 220 nm thick ZnO. (c) and (d) The calculation model of position dependence of the nonradiative damping  $\Gamma_{\sigma,i}$  for the respective thicknesses.

material parameters as follows: the transverse exciton energy  $E_{A(B)} = \epsilon_{A(B)} - 2t_{A(B)} = 3.3780$  (3.3833) eV, the LT-splitting energy  $\Delta_{LT}^{A(B)} = 3.0$  (9.9) meV, the effective mass  $M_{A(B)} = 0.87m_0$  ( $0.87m_0$ ), the background dielectric constant  $\epsilon_b = 4.95$ , and the refractive index of the sapphire substrate  $n_{\text{sapphire}} = 1.83$ . The thickness was estimated to be 289 nm for Fig. 2(a) and 220 nm for Fig. 2(b). The incident surface tended to exhibit large  $\Gamma_{\sigma,i}$ , which suppresses contributions of the surface-localized states. This relates to the well-known “dead-layer” effects [31–33], which have been used to express the strong distortion of excitonic wave functions near the surfaces. On the other hand, there are domains with relatively small  $\Gamma_{\sigma,i}$ , contributing to the peak structures around the transverse exciton energies  $E_{\sigma}$  in the reflectance [34], as well as the TG spectrum described below. For more detailed consideration of the position dependence of  $\Gamma_{\sigma,i}$ , see Ref. [35].

TG signals include the light-exciton coupled mode with radiative shift and width, and these can be understood on the basis of the size-quantized exciton model. To describe the contribution from the  $n$ th size-quantized state depicted in Fig. 1, we transform  $\langle\beta_{\sigma,i}\rangle(\omega)$  as  $A_n(\omega) = \sqrt{(2/N+1)} \times \sum_i \sin k_n i \langle\beta_{A,i}\rangle(\omega)$ ,  $B_n(\omega) = \sqrt{(2/N+1)} \sum_i \sin k_n i \langle\beta_{B,i}\rangle(\omega)$ , where  $k_n = (n\pi/N+1)$  ( $n = 1, 2, \dots, N$ ) are the quantized wave numbers of an exciton.  $A_n(\omega)$  and  $B_n(\omega)$  indicate induced polarizations associated with the  $n$ th state of  $A$  and  $B$  excitons, respectively, which include information regarding the radiative corrections. Moreover, between the same  $n$ th states of the  $A$  and  $B$  excitons, strong mixing occurs that results in the diagonalized light-exciton coupled modes [13]. TG spectral structures reflect light-exciton coupled modes with radiative correction. Hence, they can be reproduced with the induced polarizations under certain superpositions.

With the material parameters determined from the reflectance fitting, we calculated the induced polarizations  $A_n(\omega)$  and  $B_n(\omega)$  to give an interpretation of the TG spectrum. If we assume that each of the  $A$  and  $B$  excitons independently contributes to the signal, a large number of nearly degenerate states in the region between  $E_A$  and  $E_B$  bring a single peak [denoted by the dotted line in Fig. 3(a-1)]. On the other hand, the component mixing of  $A$  and  $B$  excitons results in destructive interference in this energy region, which explains the dip in the observed signal shown in Fig. 3(a-2). In addition, the broad spectral tails in the observed TG signal shown in Fig. 3(a-1) cannot be fully explained exclusively using the previously demonstrated scheme, where particular exciton states exhibit large radiative width due to the spatial phase matching with light waves beyond the LWA [15–18]. The component mixing of  $A$  and  $B$  excitons brings additional radiative broadening through constructive interference in the lower and higher energy region. By considering these two broadening mechanisms, we successfully determined attributions

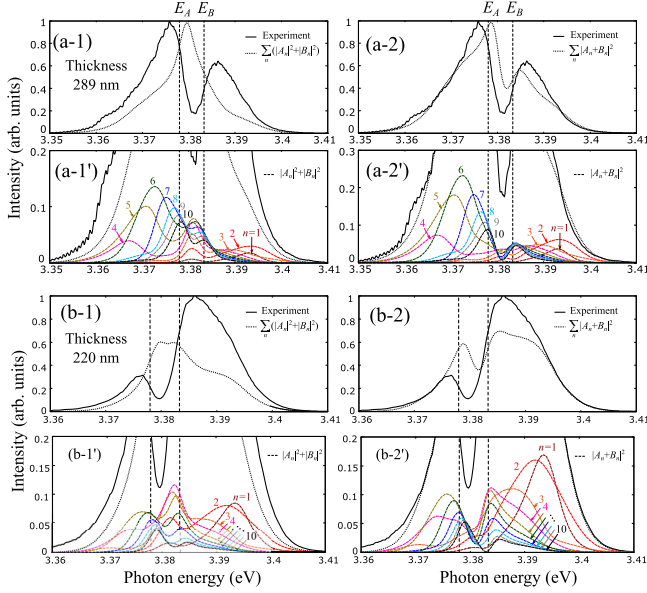


FIG. 3. (a) Fitting of the TG signal by a sum of the induced polarizations (a-1) without and (a-2) with component mixing of the  $A$  and  $B$  excitons for 289 nm thick ZnO. (b) The same for a 220 nm thick sample. (a-1'), (a-2'), (b-1'), and (b-2') show enlarged figures of the respective figures above, where induced polarizations of  $n = 1, 2, \dots, 10$ th exciton states are displayed.

of the broad spectral tails in the observed TG signal to the  $n = 1, 2$ , and 3 states, which shifted to the higher region, and the  $n = 4, 5$ , and 6 states in the lower region, as shown in Fig. 3(a-2'). The same discussion can be applied to different sample thicknesses, as shown in Fig. 3(b).

The spectral analyses motivated us to examine the decay profile of the TG signal in the broad tail regions, insofar as the radiative decay rates of excitons are expected to be greatly enhanced due to the above mechanisms. By performing the eigenmode analysis described in Ref. [13] with the material parameters determined from the reflectance fitting in Fig. 2, we theoretically obtained eigenenergies of light-exciton coupled modes. Particular coupled modes with (pure) radiative decay times in the order of 100 and 10 fs are listed in Table I. By tuning the incident lasers to the respective eigenenergies, we experimentally measured the delay-time dependence of the TG signals, as shown in Fig. 4. The measured signals contain both fast- and slow-decay components, which can be fitted by a

TABLE I. Calculated eigenenergy and radiative decay time of particular light-exciton coupled modes for 289 and 220 nm ZnO obtained by eigenmode analysis according to Ref. [13].

Thickness	Eigenenergy	Decay time	Reference to Fig. 4
289 nm	3.3571 eV	18.7 fs	(a)
	3.3685 eV	132 fs	(b)
220 nm	3.3705 eV	151 fs	(c)

double-exponential function convoluted by the excitation laser profile (solid red line). Particularly, for fast decay in the order of 10 fs, we carefully examined the fitting, as detailed in the Supplemental Material [35]. The reproduced decay profile is highly sensitive to changes to the assumed radiative decay time (by a couple of femtoseconds). The fast components correspond well to the radiative decay times obtained from the eigenmode analyses. On the other hand, the slow components are due to other multiple (slow-decay) coupled modes showing beating by two peaks in the TG spectra (arising from the coherence between  $A$  and  $B$  excitons.) Significantly, the fast decay time reaches a typical dephasing time when the semiconductors are at room temperature [24]. This means that such a fast coherent decay component will survive even at room temperature and its coherent optical response will be completed with a low heating effect because of the radiative decay nature. The presented agreement between the observed and calculated results ensures that the origins of drastic enhancements to the radiative decay rate are both the nonlocal response and the component mixing of  $A$  and  $B$  excitons via radiation fields.

The results obtained by the theoretical and experimental studies establish a highly enhanced radiative decay rate of excitons, even in real, spatially inhomogeneous ZnO samples. The considerable speedup of the radiative decay is due to the synergetic effects of the large light-exciton interaction volume beyond LWA, along with the component mixing of  $A$  and  $B$  excitons. Future studies with a

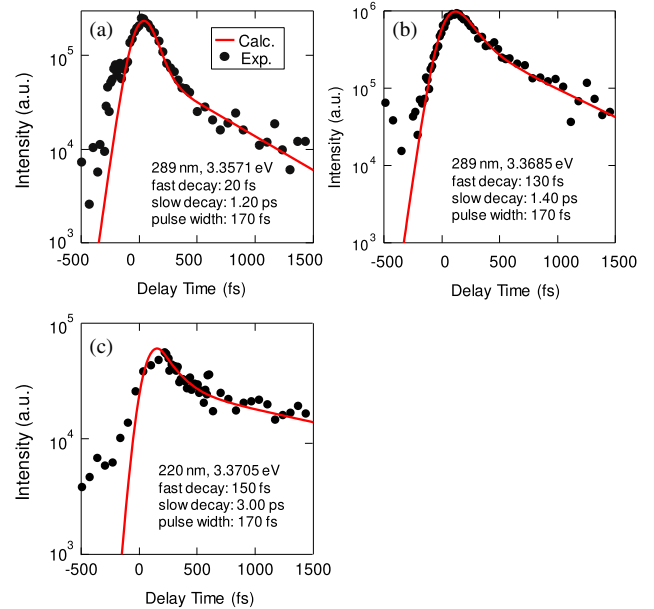


FIG. 4. Observed delay-time dependence of the TG signal at (a) 3.3571 and (b) 3.3685 eV for a 289 nm thick sample, and at (c) 3.3705 eV for a 220 nm thick sample. The solid red lines represent fitting curves by a double-exponential function convoluted by the excitation laser profile.

much shorter incident-pulse duration and a microscopic model of nonradiative damping will open the possibility of ZnO for ultrafast low-energy-loss optical devices.

The authors thank Professor N. Yokoshi for helpful discussion. This work was partially supported by a Grant-in-Aid for JSPS Fellows No. 16J11326 from MEXT, Japan, JSPS KAKENHI Grant No. 15K05133 Grant-in-Aid for Scientific Research (C), and Grant No. JP16H06504 in Scientific Research in Innovative Areas: “Nano-Material Optical Manipulation.”

T. K. and T. M. contributed equally to this work.

\*matsuda.t@issp.u-tokyo.ac.jp

Present address: Institute for Solid State Physics, University of Tokyo, Kashiwa, Chiba 277-8581, Japan.

†ishi@mp.es.osaka-u.ac.jp

- [1] D. Maryenko, A. McCollam, J. Falson, Y. Kozuka, J. Bruin, U. Zeitler, and M. Kawasaki, *Nat. Commun.* **9**, 4356 (2018).
- [2] J. Falson and M. Kawasaki, *Rep. Prog. Phys.* **81**, 056501 (2018).
- [3] C. Klingshirn, *Phys. Status Solidi (b)* **244**, 3027 (2007).
- [4] C. Klingshirn, *Chem. Phys. Chem.* **8**, 782 (2007).
- [5] M. Chen, M. P. Lu, Y. Wu, J. Song, C. Lee, M. Y. Lu, Y. Chang, L. Chou, Z. Wang, and L. Chen, *Nano. Lett.* **10**, 4387 (2010).
- [6] X. Li, J. Qi, Q. Zhang, Q. Wang, F. Yi, Z. Wang, and Y. Zhang, *Appl. Phys. Lett.* **102**, 221103 (2013).
- [7] Z. Zhang, Y. Wang, S. Yin, T. Hu, Y. Wang, L. Liao, S. Luo, J. Wang, X. Zhang, P. Ni, X. Shen, C. Shan, and Z. Chen, *Opt. Exp.* **25**, 17375 (2017).
- [8] J. J. Cole, X. Wang, R. J. Knuesel, and H. O. Jacobs, *Nano. Lett.* **8**, 1477 (2008).
- [9] J. Jean, S. Chang, P. R. Brown, J. J. Cheng, P. H. Rekemeyer, M. G. Bawendy, S. Gradečak, and V. Bulović, *Adv. Condens. Matter Phys.* **25**, 2790 (2013).
- [10] M. Zamfirescu, A. Kavokin, B. Gil, G. Malpuech, and M. Kaliteevski, *Phys. Rev. B* **65**, 161205(R) (2002).
- [11] L. Orosz, F. Réveret, F. Médard, P. Disseix, J. Leymarie, M. Mihailovic, D. Solnyshkov, G. Malpuech, J. Zuniga-Pérez, F. Semon, M. Leroux, S. Bouchoule, X. Lafosse, M. Mexis, C. Brimont, and T. Guillet, *Phys. Rev. B* **85**, 121201(R) (2012).
- [12] F. Li, L. Orosz, O. Kamoun, S. Bouchoule, C. Brimont, P. Disseix, T. Guillet, X. Lafosse, M. Leroux, J. Leymarie, G. Malpuech, M. Mexis, M. Mihailovic, G. Patriarche, F. Réveret, D. Solnyshkov, and J. Zuniga-Perez, *Appl. Phys. Lett.* **102**, 191118 (2013).
- [13] T. Kinoshita and H. Ishihara, *Phys. Rev. B* **94**, 045441 (2016).
- [14] T. Kinoshita and H. Ishihara, *Phys. Rev. B* **95**, 155418 (2017).
- [15] H. Ishihara, K. Cho, K. Akiyama, N. Tomita, Y. Nomura, and T. Isu, *Phys. Rev. Lett.* **89**, 017402 (2002).
- [16] H. Ishihara, J. Kishimoto, and K. Sugihara, *J. Lumin.* **108**, 343 (2004).
- [17] A. Syouji, B. P. Zhang, Y. Segawa, J. Kishimoto, H. Ishihara, and K. Cho, *Phys. Rev. Lett.* **92**, 257401 (2004).
- [18] M. Ichimiya, M. Ashida, H. Yasuda, H. Ishihara, and T. Itoh, *Phys. Rev. Lett.* **103**, 257401 (2009).
- [19] M. Takahata, K. Tanaka, and N. Naka, *Phys. Rev. Lett.* **121**, 173604 (2018).
- [20] G. T. Noe II, J. Kim, J. Lee, Y. Wang, A. K. Wójcik, S. A. McGill, D. H. Reitze, A. A. Belyanin, and J. Kono, *Nat. Phys.* **8**, 219 (2012).
- [21] T. Laurent, Y. Todorov, A. Vasanelli, A. Delteil, C. Sirtori, I. Sagnes, and G. Beaudoin, *Phys. Rev. Lett.* **115**, 187402 (2015).
- [22] F. Jahnke, C. Gies, M. Aßmann, M. Bayer, H. A. M. Leymann, A. Foerster, J. Wiersig, C. Schneider, M. Kamp, and S. Höfling, *Nat. Commun.* **7**, 11540 (2016).
- [23] C. Poellmann, P. Steinleitner, U. Leierseder, P. Nagler, G. Plechinger, M. Porer, R. Bratschitsch, C. Schüller, T. Korn, and R. Huber, *Nat. Mater.* **14**, 889 (2015).
- [24] P. C. Becker, H. L. Fragnito, C. H. B. Cruz, R. L. Fork, J. E. Cunningham, J. E. Henry, and C. V. Shank, *Phys. Rev. Lett.* **61**, 1647 (1988).
- [25] D. W. Phillion, D. J. Kuizenga, and A. E. Siegman, *Appl. Phys. Lett.* **27**, 85 (1975).
- [26] T. Yajima and H. Souma, *Phys. Rev. A* **17**, 309 (1978).
- [27] T. Yajima, H. Souma, and Y. Ishida, *Phys. Rev. A* **17**, 324 (1978).
- [28] H. J. Carmichael, *Statistical Methods in Quantum Optics I Master Equations and Fokker-Planck Equation* (Wiley-IEEE Press, New York, 1995).
- [29] W. C. Chew, *Waves and Fields in Inhomogeneous Media* (Springer-Verlag, Berlin, Heidelberg, 1999).
- [30] M. Nakayama, S. Komura, T. Kawase, and D. Kim, *J. Phys. Soc. Jpn.* **77**, 093705 (2008).
- [31] J. J. Hopfield and D. G. Thomas, *Phys. Rev.* **132**, 563 (1963).
- [32] F. Evangelisti, A. Frova, and F. Patella, *Phys. Rev. B* **10**, 4253 (1974).
- [33] V. A. Fonoberov and A. A. Balandin, *Phys. Rev. B* **70**, 195410 (2004).
- [34] In the case of GaAs thin films, it was reported that only the top layer has considerably small damping ( $\Gamma = 0.03$  meV) among the threefold layers [15]. Although our growth method differs from that described in Ref. [15], our fitting for ZnO thin films reveals another example of the similar effect of forming position-dependent nonradiative damping.
- [35] See Supplemental Material at <http://link.aps.org/supplemental/10.1103/PhysRevLett.122.157401> for detailed descriptions on the fitting of (I) the linear reflectance spectra and (II) the TG time profiles.